The architecture of submarine monogenetic volcanoes – insights from 3D seismic data

P. Reynolds[1*], N. Schofield[2], R.J. Brown[3], S. Holford[1]

[1] Centre for Tectonics, Resources and Exploration (TRaX), Australian School of Petroleum, University of Adelaide, Adelaide, SA 5005, Australia

[2]Department of Geology & Petroleum Geology, University of Aberdeen, Aberdeen AB24 3UE, UK

[3] Department of Earth Sciences, Durham University, Science Labs, Durham, DH1 3LE, UK

*Corresponding author: peter.reynolds@adelaide.edu.au, +61484607355

Abstract

Many prospective sedimentary basins contain a variety of extrusive volcanic products that are ultimately sourced from volcanoes. However, seismic reflection-based studies of magmatic rift basins have tended to focus on the underlying magma plumbing system, meaning that the seismic characteristics of volcanoes are not well understood. Additionally, volcanoes have similar morphologies to hydrothermal vents, which are also linked to underlying magmatic intrusions. In this study, we use high resolution 3D seismic and well data from the Bass Basin, offshore southern Australia, to document 34 cone- and crater-type vents of Miocene age. The vents overlie magmatic intrusions and have seismic properties indicative of a volcanic origin: their moderate–high amplitude upper reflections and zones of "wash-out" and velocity pull-up beneath. The internal reflections of the vents are similar to those found in lava deltas, suggesting they are composed of volcaniclastic material. This interpretation is corroborated by data from exploration wells which penetrated the

flanks of several vents. We infer that the vents we describe are composed of hyaloclastite and pyroclasts produced during submarine volcanic eruptions. The morphology of the vents is typical of monogenetic volcanoes, consistent with the onshore record of volcanism on the southern Australian margin. Based on temporal, spatial and volumetric relationships, we propose that submarine volcanoes can evolve from maars to tuff cones as a result of varying magma-water interaction efficiency. The morphologies of the volcanoes and their links to the underlying feeder systems are superficially similar to hydrothermal vents. This highlights the need for careful seismic interpretation and characterization of vent structures linked to magmatic intrusions within sedimentary basins.

1. Introduction

Many magmatic rift basins are characterised by mafic volcanism, which produces a combination of both extrusive and intrusive components. Extrusive components include vent-like features that are volcanic (e.g. Bell & Butcher, 2002; Davies *et al*., 2005; Thomson, 2007; Wall *et al.,* 2010; Calvès *et al*., 2011; Jackson, 2012; Magee *et al*., 2013b; Zhao *et al*., 2014; Schofield *et al*., 2015) or hydrothermal in origin (e.g. Jamtveit *et al*., 2004; Svensen *et al*., 2004; Planke *et al.* 2005; Hansen, 2006; Grove, 2013; Magee *et al*., 2013a; Magee *et al*., 2013b; Magee *et al*., 2015; Alvarenga *et al*., 2016). However, the criteria for distinguishing these vents in seismic data were until now lacking.

Volcanoes are composed of either fragmental or coherent volcanic rock. They link the extrusive and intrusive components of volcanic provinces and in-part determine their architecture (e.g. Valentine & Cortés 2013; Re *et al*., 2015). Their eruption mechanisms vary from magmatic volatile-dominated (eruptions resulting from the expansion of magmatic volatiles) to phreatic (heating of ground or surface water by magma) and phreatomagmatic (resulting from the physical mixing of ground or surface water with magma) (Sigurdsson *et al*., 2015). Volcanoes can be used to identify structural trends, stratigraphic relationships and feeder systems that can be difficult to image in seismic data; thus providing insights into the subsurface geology (e.g. Ebinger *et al*., 1989; Connor & Conway, 2000; Schofield *et al*., 2015). They also have the potential to act as hydrocarbon reservoirs, since the volcaniclastic rocks of which many volcanoes are composed can have high permeabilities and porosities (e.g. Magara, 2003; Schutter 2003; Holford *et al.,* 2012).

Hydrothermal vents have eye, dome or crater-like shaped upper parts (Planke *et al.* 2005; Grove, 2013) underlain by a sandstone dyke or breccia pipe that connects at depth to the tips of a sill (Jamtveit *et al*., 2004). Based on observations from seismic data, these connection zones have confusingly been referred to as diatremes (Hansen, 2006) a feature diagnostic of volcanoes (White & Ross, 2011). Hydrothermal vents may act as fluid migration pathways long after their burial (Svensen *et al*., 2003). Moreover, their upper parts may represent a hydrocarbon play (Grove, 2013). The vents have been interpreted to arise from either phreatic or phreatomagmatic activity (Jamtveit *et al*., 2004) yet there are no descriptions of the juvenile clasts indicative of a phreatomagmatic origin.

Well data indicates hydrothermal vents are dominantly composed of remobilised sediment sourced from above the sill, which is subsequently effused from a central vent during a series of pulses (Grove, 2013). The upper parts of hydrothermal vents from the North Atlantic are composed of disaggregated gravel to silt-sized clasts of quartz, woody fragments, pelagic sediments and minor carbonaceous debris (Grove, 2013). Well data from other vent complexes indicates they are composed of diatomitic siltstone with carbonate layers (Svensen *et al*., 2003) and sandstone, sediment breccia and claystone (Svensen *et al*., 2006). Some vents also contain clasts of dolerite thought to be sourced from an intrusion (Grove, 2013) although the genesis (e.g. magma-sediment interaction or hydroclastic fragmentation) and source of the clasts (e.g. the allied or a superjacent intrusion) is not described. Volumetrically minor components of volcanic clasts have also been documented from boreholes drilled through the breccia pipes in the Karoo (Svensen *et al*., 2007).

The main concentrations of these clasts occur close to the sill (Svensen *et al.*, 2007); whether these "mixtures" of volcanic and sedimentary material result from magma-sediment interaction or otherwise is unclear.

Given the similar morphologies of hydrothermal vents and volcanoes, their similar location within volcanic provinces, and their relationship to underlying sills, it has proved difficult to distinguish between them. For instance, based on observations of the feeder system, early workers proposed that some hydrothermal vents within the Karoo are almost wholly composed of volcanic material (Jamtveit *et al.*, 2004 and references there-in). However, later work revealed that these features represent feeders for volcanoes formed during phreatomagmatic activity (McClintock *et al.*, 2008). In seismic data, the origin of some vents has only been confirmed following drilling (Davies *et al.*, 2002; Grove, 2013). Further hampering the identification of volcanoes is the fact that monogenetic volcanoes display a variety of morphologies, some of which are unresolvable due to their height and basal diameter being below the vertical resolution and line spacing of 2D seismic surveys.

This study uses 3D seismic and well data to describe the facies architecture of Miocene-aged submarine volcanoes formed offshore southern Australia. These volcanoes are found at shallow depths (1208 metres below sea floor) and are free from overlying basalt cover, making them ideal candidates for study. We provide a detailed assessment of their architecture, allowing us to highlight the criteria for distinguishing between types of vents in seismic data. We also provide insights into how their morphologies varied as a result of varying magma-water mixing.

2. Geological setting and Dataset

The southern margin of Australia formed as a result of Gondwanan rifting that commenced in the Middle−Late Jurassic, culminating in breakup in the Campanian (Totterdell & Bradshaw, 2004).

The margin is characterised by a series of east-west trending rift basins and an abundance of both offshore and onshore intraplate igneous rocks (e.g. Holford *et al.*, 2012; Ball *et al.,* 2013). Magmatism has been linked to late-stage rifting processes at a craton margin (Ball *et al.,* 2013), impingement of a mantle plume (Davies *et al.,* 2015) or shear- and edge-driven mantle convection (Meeuws *et al.*, 2016). Many of the volcanoes are monogenetic in origin, and range from Jurassic to Recent in age (Johnson, 1989; Cas *et al.*, 1993). Onshore volcanism in the Newer Volcanic Province, southern Australia, is characterised by maars, scoria cones, tuff cones and lava flows, produced during subaerial and submarine volcanic activity (Cas *et al.*, 1993). Despite the abundance of volcanism, the margin is classified as magma-poor due to the late stage arrival of relatively low volumes of magma (Norvick & Smith, 2001; Sayers *et al.,* 2001; Holford *et al.,* 2012; Ball *et al.,* 2013).

The Bass Basin is located offshore between Victoria and northern Tasmania (Fig. 1). It represents a failed intra-cratonic rift basin (Blevin, 2003) and consists of a series of Cretaceous northwest-southeast trending half-grabens (Holford *et al.*, 2012). As summarised by Blevin (2003), the basin fill is characterised by a transgressional sequence, developing from a terrestrial sequence in the Mid Eocene to shallow marine in the present day. Fluvio-lacustrine sequences are found in the Late Cretaceous to Mid Eocene, characterised by the Eastern View Coal Measures (EVCM). Marine transgression continued from the Middle Eocene onwards, forming an estuarine and shallow marine embayment. The overlying Oligocene and Miocene Torquay Group is composed of shallow marine marl and limestone, deposited during continued sea level rise.

The Bass Basin also contains a variety of Cretaceous–Miocene-aged igneous features, many of which have been penetrated by petroleum exploration wells (Holford *et al.,* 2012; Table 1). The oldest are Cretaceous volcaniclastic sandstones, although the source of these is unclear (Holford *et al.,* 2012). Subsequent Mid-Cretaceous volcanism produced a series of volcanoes, flows and sills (Blevin, 2003; Trigg *et al.*, 2003; Holford *et al.*, 2012). Volcanism peaked in the Palaeocene and

Oligocene-Miocene, evidenced by widespread lavas, sills and dykes found through the central and north-east Bass Basin (Blevin, 2003).

This study utilises 3D seismic data from the Yolla and Labatt marine surveys which were acquired in 1994 and 2008 respectively. These surveys were acquired with streamer lengths of 3 km and 6 km. We use the PreStack Time Migrated data displayed with SEG Normal polarity. The 525 km^2 Labatt survey has a bin size of 25 × 12.5 m. The Yolla survey is smaller, covering 260 km^2 with a 25 x 12.5 m bin size. A 2D seismic line is used to tie these two surveys (section A–A´, Figs. 1 and 2) and also intersects the Bass-1 well which penetrates the flanks of a vent.

3. Methodology

The vents occur at three separate levels within the Miocene succession of the Bass Basin (Fig. 2). We therefore mapped three pairs of Base and Top Volcanic surfaces which bound the vents, which are numbered according to their stratigraphic position. The vents in the Yolla survey are oldest and occur towards the base of the Miocene Torquay Group; these are the TV1 and BV1 horizons which have been tied using a synthetic seismogram from the Yolla-1 well. This well penetrated 68 m of volcanic rocks between 1237 and 1305 m (Fig. 3). The vents in the Labbatt survey, which are not penetrated by wells, have been mapped using the TV2 and BV2 horizons (Fig. 2). The youngest vents occur within sediments of mid-late Miocene age, and have been mapped using the TV3 and BV3 horizons. These horizons are tied to the Bass-1 well, which penetrated 160 m of volcanic rocks between 790 and 950 m (Fig. 3). Horizons TV1, TV2 and TV3 are peak events that define the onlap surface of the vents and vary from moderate to high amplitude. The dominant frequency at the TV2 horizon is 45 Hz and the dominate frequency of the TV1 is 39 Hz, indicating the vertical resolution is 15−20 m in the Labatt and Yolla surveys respectively. The BV1−BV3 horizons are trough events that define the horizon downlapped by the vents' internal reflections, and vary from high to low amplitude. The horizons are mapped locally beneath the vents and are often poorly imaged beneath their central parts. Detailed mapping of the TV2, BV2 and TV1 and BV1 horizons allowed us to investigate the distribution and morphology of the vents in the Labbatt (Figs. 4 and 5) and Yolla surveys respectively (Figs. 4 and 6).

Many of the vents are underlain by seismic velocity pull-ups (Fig. 2). The height of the velocity pull-up relative to the regional base datum was used to calculate the internal velocity of each vent, using the method defined by Magee *et al.* (2013b). This gave each vent a value of between 2200 and 4025 m s^{-1} (assuming a velocity of 2090 m s^{-1} for the Miocene Torquay Group; as constrained from Yolla-1 well data). Where pull-ups were absent beneath a vent, a velocity of 2090 m s^{-1} was used. These velocities were used to calculate the vent heights and are accurate to within 100 m (allowing for a velocity variation of 600 m s^{-1} within the Miocene Torquay Group).

The Labatt survey contains several sills (Fig. 4). These are recognised by high amplitude, continuous reflections that cross cut adjacent reflections (e.g. Thomson & Hutton, 2004; Holford *et al.*, 2012). The dominant frequency at the depths at which the sills are found is ~40 Hz in both surveys, suggesting the sills need to be >30 m thick to be resolved and >13 m thick to be detected. We use a velocity of 3000 m s^{-1} (as constrained from the Bass-1 well; see Trigg *et al.*, 2003) to calculate the depth of the sills beneath the BV2 horizon.

4. Vent characteristics

4.1 Vent morphology

The vents can be categorised into cone- and crater-types according to their morphology (Fig. 7; Table 2). The crater-types (Fig. 7A) are represented by sub-circular excavations in the TV2 surface which range from 340−1200 m in diameter, and are underlain by <300 m wide, funnel-shaped features that extend 50−100 m into the subsurface. The crater-type vents are only found in the

Labatt survey. Their craters are filled with low amplitude, sub-horizontal reflections which onlap the crater margins and are surrounded by concentric faults. The cone-type vents, which are found in both surveys, include: 1) pointed; 2) cratered, and 3) flat topped morphologies. These vents have sub-circular bases, are roughly symmetrical in plan view and have a distinctive onion-ring structure in time slice. Their flanks dip 5–18° and their basal diameter and height increases as their volume increases (Fig. 7E and F). The pointed vents have a conical morphology (Fig. 7B). They overlie the crater-type vents. The cratered vents (Fig. 7C) are characterised by an upper bowl-shaped reflection that defines a ~30 m deep crater in the centre of the edifice. The flat-topped vents (Fig. 7D) lack craters and instead have sub-horizontal tops.

4.2 Seismic facies

Internally, the cone-shaped vents are composed of two differing seismic facies which are distinguished on the basis of the reflection amplitude, morphology and facies geometry. Seismic facies 1 (SF1) is composed of moderate to high amplitude reflections with a hummocky character (Fig. 7B–D). They only occur within the vent flanks. The reflections vary from semi-continuous to continuous and form wedge-shaped packages ≤0.2 s thick. They are oriented sub-parallel to the TV1 and TV2 horizons. The facies downlaps the BV1 and BV2 horizons and progrades laterally from the centre of the vent which is commonly composed of seismic facies 2 (SF2). This facies is composed of low amplitude, discontinuous reflections that grade laterally into SF1. SF2 forms plug-like bodies up to 2 km wide in the central part of the vents (Fig. 7B–D). This facies is oriented oblique to the TV1 and TV2 horizons and may truncate the BV1 and BV2 horizons, extending beneath the vents for ≤0.2 s.

The reflections overlying the vents are sub-parallel in orientation and have low amplitudes. Polygonal faulting is observed in a ~0.1 s-thick sequence of reflections overlying the vents at ~0.6 s and ~0.8 s in the Labatt and Yolla surveys respectively. The reflections are commonly domed above the vents (Figs. 2, 5 and 6) and are disrupted by vertical pipe-like features above the summit of the vent drilled by the Yolla-1 well (Fig. 6).

4.3 Spatial Distribution

Within both the Labatt and Yolla surveys, the vents form linear rows, or occur as isolated vents (Figs. 5 and 6). Those in rows are spaced 800–3000 m apart and contain up to four individual vents, which onlap in a northerly direction and decrease in volume towards the south. The rows are oriented approximately north-south, and overlie north-south oriented grabens. 23% of the isolated vents do not overly faults, while the remaining 77% are found above the upper tips of normal faults.

Sills are only found beneath the isolated vents within the Labatt survey. They occur 500−1200 m beneath 8% of the vents. These sills have a saucer- or layer-parallel shape and range from 2–4 km in diameter. They occur as isolated bodies and do not form vertically interconnected complexes with adjacent sills. The sills have tips which shallow beneath the centres of the vents (Fig. 8). The sills are connected to the overlying vents by a zone of velocity pull-up roughly equal in width to that of the vent. No evidence of forced folding is observed above the sills. The remaining 92% of the vents are not visibly connected to an underlying sill and are underlain by regions of poor imaging and velocity pull-up.

5. Interpretation

5.1 Environment of formation

The vents are interpreted to have formed in a shallow marine environments, evidenced by the transgressional sequence within which the vents are found and the overlying marls and limestones (e.g. Boreen & James, 1995). An extrusive origin for the cone-shaped vents is indicated by the reflections which onlap the vents, and the reflections within the vents which downlap the underlying horizon. The doming of reflections above the vents is typical of differential compaction, suggesting that the vents are composed of denser rock than the overlying sediments. The fact that the vents are found at different stratigraphic levels (Fig. 2) clearly indicates that vent formation was not synchronous across the Bass Basin.

5.2 Preservation of the vents

The cone-type vents are not interpreted to be the erosional "stumps" of larger edifices, since the vents retain no evidence for erosion such as wave-cut platforms or erosional rills and gullies. Furthermore, they preserve features such as craters (e.g. Fig. 7C) that suggest they are preserved in a near-pristine state. Other vents along the southern Australian margin constructed in a submarine environment are similarly preserved in a near-pristine state; Jackson (2012) attributes this to 1) rapid flooding of the vents during eustatic sea level rise; 2) the location of the vents on the outer shelf, reducing wave and tidal erosion; 3) weak post-Eocene ocean currents, and 4) no caldera collapse. We infer similar processes for the vents in this study, and highlight also that caldera collapse is only typical of large polygenetic volcanoes, unlike the vents in this study (see following section).

5.3 Evidence for a volcanic origin

Numerous exploration wells within the Bass Basin have penetrated intrusive and extrusive volcanic rocks identified in wireline logs, cuttings and sidewall cores (Table 1). For example, the Bass-1 well was drilled to test the hydrocarbon potential of a Miocene "reef complex". This reef complex was subsequently shown to be a volcano, as the well intersected a 160 m-thick sequence of volcanic rocks interpreted as pyroclastic deposits (Blevin, 2003; Trigg *et al.*, 2003). The Yolla-1 well also intersected a 68 m-thick sequence of fragmental volcanic rock, interpreted to represent highly altered pyroclastic deposits (Blevin, 2003). This indicates that the vents are volcanic in origin.

The seismic characteristics of the vents are also typical of volcanic lithologies; the TV1 and TV2 horizons are high amplitude relative to the overlying reflections (Figs. 5 and 6). This indicates that the TV1 and TV2 surfaces represent a high acoustic impedance boundary. The cone-shaped vents also produce pull-up features beneath them; typical of volcanic rocks within a sedimentary sequence (Jackson, 2012; Magee *et al.*, 2013b). The calculated velocities of the vents (section 3) is higher than that reported for hydrothermal vents (<1800 m s^{-1}; see Svensen *et al.*, 2003) yet lower than that of lava flows (commonly 3300–6800 m s^{-1}; see Planke & Eldholm, 1994; Nelson *et al.*, 2009). This suggests that the cone-shaped vents are dominantly composed of fragmental, volcaniclastic material (e.g. pyroclasts and hyaloclastite) as opposed to lavas that typify effusive, subaerial volcanic eruptions, or sands and silts that typify hydrothermal vents (e.g. Grove 2013).

Volcaniclastic deposits such as pyroclasts and hyaloclastite are typical products of submarine eruptions (e.g. Kokelaar, 1986; Suiting & Schmincke, 2009; Watton *et al.*, 2013a), consistent with the interpreted emplacement environment of the vents. Hyaloclastite has variable grain sizes and vesicularities (e.g. Watton *et al.*, 2013a; Watton *et al.*, 2013b). These properties affect the velocity and hence seismic amplitude of the component facies, and could produce a seismic reflection of moderate or high amplitude, such as that which typifies the TV1 and TV2 horizons. Facies similar to SF1 which typify the flanks of the vents are reported in other seismic datasets from volcanic margins, and represent hyaloclastite at the fronts of lava deltas (e.g. Planke *et al.*, 2000; Wright *et al.*, 2012). Poor imaging in regions represented by SF2 may result from the high impedance contrast of the TV1 and TV2 horizons. Furthermore, this central region may contain numerous dykes intruded into the edifice, creating high velocity contrast between fragmental and coherent volcanic material.

Our interpretation that the vents are volcanic in origin is consistent with the long-lived, episodic record of magmatism onshore. The southern margin of Australia has experienced volcanic activity since the Jurassic to the near present day, much of which is monogenetic in origin. Miocene examples of pillow lavas and submarine basalts outcrop on the northern coast of Tasmania (Fox *et* al., 2016) whilst the most recent expression of volcanism along the margin is found in the Newer Volcanic Province (aged 4.5 Ma to 4.5 kyr) in Victoria. This province is typified by over 400 tuff cones, lava flow, maars and scoria cones (Boyce *et al.*, 2014). Here and elsewhere along the onshore southern Australian margin, no hydrothermal vents are recognised.

The vents in our study also share many morphological characteristics with volcanoes. The volumes of the cone and crater-type vents are typical of monogenetic volcanoes (commonly <1 km^3; see White & Ross, 2011). The distance at which the vents are spaced in linear rows is also typical of volcanoes aligned along fissures (Thordarson & Self, 1993). The pit craters have similar dimensions to maars; these are explosion craters in the country rock with diameters of 0.2−3 km (White & Ross, 2011). The funnel-shaped conduits beneath the pit craters have similar dimensions and morphologies to diatremes, which underlie maars (White & Ross, 2011). The ejecta rings that surround maars are commonly <30 m in height and are not recognised, perhaps due to altered depositional regimes in the submarine environment. The pointed vents are interpreted to be pillow volcanoes (Batiza & White, 2000) a type of submarine volcano that forms during the subaqueous effusion of basaltic lava. Pillow volcanoes are of similar dimensions to the pointed edifices and similarly lack a crater (Batiza, & White, 2000). They are composed of volcaniclastic material (hyaloclastite and pillow lavas). Pillow volcanoes represent the early stages of tuff cone growth (e.g. Moore, 1985). The cratered and flat-topped edifices are interpreted as monogenetic tuff cones on the basis of their similar size and similar crater dimensions (White & Ross, 2011). Tuff cone-forming eruptions may effuse lava in the later stages (Moore, 1985) and the flat topped vents are interpreted as tuff cones within which lavas and/or hyaloclastite has filled their crater.

The facies and architecture of the vents identified in this study are broadly similar to those of the submarine volcanoes and shield volcanoes described by Bell & Butcher (2002) and Magee *et al.* (2013b). These volcanoes have onion ring structures in plan view, high amplitude tops and prograding reflections in their flanks. Zhao *et al.* (2014) describe "volcanic mounds" from the South China Sea, which have a similar size and depth relationship to sills to the vents we describe. However, these features lack detailed description to provide further comparison. The pit craters have a similar size, and morphology to the maars described by Wall *et al.* (2010), in which dykes are clearly imaged beneath the maar using magnetic data.

The spatial relationship between the sills and vents suggests that the sills acted as feeders for the vents (Fig. 8). Furthermore, the intrusion penetrated by the Cormorant-1 well (Table 1) was of Miocene age (Sutherland & Wellman, 1986) suggesting that the vents and sills are temporally related. Our hypothesis is supported by other datasets which also indicate that sills can act as feeders for eruptions (Muirhead *et al.*, 2016). The vents that lack underlying sills are interpreted to have been fed by dykes, which are difficult to image in seismic datasets due to their sub-vertical orientation and narrow width (<several metres). Beneath the crater-type vents, these dykes are inferred to have transitioned into diatremes in the shallowest subsurface (i.e. less than a hundred metres). Similar feeder relationships are inferred beneath other submarine volcanoes (e.g. Suiting & Schmincke, 2012). Since there are few sills within the dataset, we infer that dykes formed the dominant mechanism of magma transport to the paleosurface. Our data supports other studies which infer that dykes play the dominant role in transporting magma to the surface in monogenetic volcanic fields, both along parts of the southern Australian margin (e.g. Holt *et al.*, 2013) and in other monogenetic volcanic fields (e.g. Muirhead *et al.*, 2016).

6 Discussion

6.1 Temporal evolution of the vents

We infer that the mapped Bass Basin vents represent ancient volcanoes "frozen" at different stages of their development, allowing for the evolution of the volcanoes to be established from an early of stage formation through to late stage full vent construction (Fig. 7). This interpretation is supported by superposition relationships and volume trends. The pit craters are directly overlain by pointed vents, indicating that the pit craters formed first. The cratered and flat-topped types are generally of larger volume than the pointed vents. We infer that the cratered and flat-topped vents represent older vents preserved in later stages of their evolution. The volcanoes may thus begin as maar-diatreme complexes on the seafloor (represented by the crater-type vents) in which magma fragmentation occurred beneath the subsurface (Fig. 9A). Continued magma supply is inferred to have led to the construction of the pillow volcanoes (represented by the pointed vents; see Fig. 9B). Growth of the volcanoes towards the sea surface resulted in the formation of tuff cones (represented by the cratered vents; Fig. 9C). The late-stage ponding of lavas and/or hyaloclastite within the tuff cone craters formed the flat-topped volcanoes.

6.2 Potential for the misidentification of volcanoes as hydrothermal vents

Volcanic-affected basins contain a range of vents which can be hydrothermal or volcanic in origin (e.g. Fig. 10; Table 3). Both types of vents form mound-shaped features on the pre-eruptive surface (Fig. 10), have similar volumes and dimensions (e.g. Planke *et al.,* 2005) and occur in linear rows (e.g. Grove, 2013). Additionally, both volcanoes and hydrothermal vents may be underlain by narrow chimney zones (Fig. 10) that connect to underlying sills at 0.7−3 km depth. Despite these similarities, our study has shown that well data and detailed seismic mapping can be used to distinguish between these types of vents.

The Bass-1 and Yolla-1 wells indicate that the volcanoes within the Bass Basin are composed of volcaniclastic material with seismic velocities of 2090–4025 m s^{-1}. In comparison, hydrothermal vents along the Northeast Atlantic margin have seismic velocities of 1800 m s^{-1} and their upper parts are composed of diatomitic siltstone, carbonate and sandstone (Svensen *et al.*, 2003; Grove, 2013). In basins which lack wells penetrating the upper parts of vents, we suggest seismic facies analysis can be used to distinguish between volcanoes and hydrothermal vents. The volcanoes we describe have moderate-high amplitude upper reflections (the TV1 and TV2 horizons) unlike the Top Vent reflections of hydrothermal vents which are low-moderate amplitude (Fig. 10). Internally, the volcanoes we describe have moderate-high amplitude hummocky reflections (SF1) in their flanks, unlike the layer-parallel, low-moderate amplitude reflections within the flanks of hydrothermal vents (e.g. Fig. 10). Additionally, the eye-type hydrothermal vents described by Planke *et al.* (2005) have inwardly dipping reflections in their lower parts, unlike the cone-shaped volcanoes in this study. Moreover, the volcanoes we describe have zones of seismic velocity pull-up beneath them (Fig. 10), a feature unreported for hydrothermal vents. It is also important to note that not all the volcanoes we describe are linked to sills, and most are interpreted to have been fed by dykes (see section 5.1). This spatial association is unlike that of hydrothermal vents, which are most commonly associated with mafic sills (e.g. Svensen *et al.*, 2004; Planke *et al.* 2005; Hansen., 2006; Grove, 2013; Magee *et al.*, 2013a; Schofield *et al.*, 2015; Alvarenga *et al.*, 2016).

Our mapping of the TV1, TV2 and TV3 horizons also indicates that multiple episodes of vent formation occurred within the Bass Basin. This is typical of onshore volcanic activity in the Newer Volcanics Province, where volcanism occurred from the Miocene through to the Holocene, producing over 400 volcanoes (Boyce *et al.*, 2014) and no hydrothermal vents. In contrast, hydrothermal vents along the northeast Atlantic margin are commonly found at a consistent stratigraphic level (Svensen *et al.*, 2004). We therefore suggest that the timing of vent formation within a basin can also help to distinguish between volcanoes and hydrothermal vents.

Whilst the lithology of the cone-shaped vents and the character of their seismic reflections enable them to be distinguished from hydrothermal structures, determining the origin of crater-type vents is more difficult. Seismic data is typically unable to image the dykes that underlie maars (cf. Wall *et al.,* 2010) and both maars and hydrothermal vents produce excavations at the paleo-surface due to blow-out of material. The association of maars with cone-shaped volcanoes, such as described in this study, may help distinguish these features in other data sets.

7. Summary

The southern margin of Australia is typified by monogenetic, intraplate volcanism. We use 3D seismic and well data from the Bass Basin, offshore northern Tasmania, to detail the architecture of Miocene-aged submarine monogenetic volcanoes. The seismic characteristics of the volcanoes are typical of volcaniclastic material, suggesting that they are composed of hyaloclastite and/or pyroclasts, consistent with descriptions from well reports. The volcanoes evolved from crater-type to cone-shaped vents perhaps as a consequence of variations in the efficiency of magma-water interaction. We highlight that the morphology of the volcanoes are superficially similar to those reported for hydrothermal vents documented from other volcanic-affected basins. We suggest the internal seismic facies of vent structures, their lithology, relationship to the magma plumbing system and the diachroneity of their emplacement can be used to determine the genesis of vents in other datasets.

Acknowledgements

Clayton Grove and Joe Cartwright are thanked for constructive reviews and Cynthia Ebinger is thanked for editorial handling. IHS Kingdom is thanked for software. Hess Company are thanked for funding through the Volcanic Margins Research Consortium.

Conflict of Interest

No conflict of interest declared.

8. References

ALVARENGA, R., IACOPINI, D., KUCHLE, J., SCHERER, C. & GOLDBERG, K. (2016) Seismic Characteristics and Distribution of Hydrothermal Vent Complexes in the Cretaceous Offshore Rift Section of the Campos Basin, Offshore Brazil. *Marine and Petroleum Geology*.

BALL, P., EAGLES, G., EBINGER, C., MCCLAY, K. & TOTTERDELL, J. (2013) The Spatial and Temporal Evolution of Strain During the Separation of Australia and Antarctica. *Geochemistry, Geophysics, Geosystems*, **14,** 2771-2799.

BATIZA, R. & WHITE, J.D.L. (2000) Submarine Lavas and Hyaloclastite. In: *Encyclopedia of Volcanoes* (Ed. by H. Sigurdsson). Academic Press.

BELL, B. & BUTCHER, H. (2002) On the Emplacement of Sill Complexes: Evidence from the Faroe-Shetland Basin. *Geological Society, London, Special Publications*, **197,** 307-329.

BLEVIN, J. (2003) (Compiler) Petroleum Geology of the Bass Basin - Interprertation Report, an Output of the Western Tasmanian Regional Minerals Program. . *Geoscience Australia, Record 2003/19*, ISSN: 1448-2177.

BOREEN, T.D. & JAMES, N.P. (1995) Stratigraphic Sedimentology of Tertiary Cool-Water Limestones, Se Australia. *Journal of Sedimentary Research*, **65**.

Boyce, J., Keays, R., Nicholls, I. & Hayman, P. (2014) Eruption Centres of the Hamilton Area of the Newer Volcanics Province, Victoria, Australia: Pinpointing Volcanoes from a Multifaceted Approach to Landform Mapping. *Australian Journal of Earth Sciences*, **61,** 735-754.

Calvès, G., Schwab, A.M., Huuse, M., Clift, P.D., Gaina, C., Jolley, D., Tabrez, A.R. & Inam, A. (2011) Seismic Volcanostratigraphy of the Western Indian Rifted Margin: The Pre-Deccan Igneous Province. *Journal of Geophysical Research: Solid Earth (1978–2012)*, **116**.

Cas, R., Satō, H. & Simpson, C.J. (1993) Newer Volcanics Province-Processes and Products of Phreatomagmatic Activity: Iavcei, Canberra 1993: Excursion Guide. *Australian Geological Survey Organisation*.

Connor, C.B. & Conway, F.M. (2000) Basaltic Volcanic Fields. *Encyclopedia of volcanoes***,** 331-343. (Ed. by H. Sigurdsson). Academic Press.

Davies, R., Bell, B.R., Cartwright, J.A. & Shoulders, S. (2002) Three-Dimensional Seismic Imaging of Paleogene Dike-Fed Submarine Volcanoes from the Northeast Atlantic Margin. *Geology*, **30,** 223-226.

Davies, R.J., MacLeod, C.J., Morgan, R. & Briggs, S.E. (2005) Termination of a Fossil Continent-Ocean Fracture Zone Imaged with Three-Dimensional Seismic Data: The Chain Fracture Zone, Eastern Equatorial Atlantic. *Geology*, **33,** 641-644.

Davies, D., Rawlinson, N., Iaffaldano, G. & Campbell, I. (2015) Lithospheric Controls on Magma Composition Along Earth/'S Longest Continental Hotspot Track. *Nature*, **525,** 511-514.

Ebinger, C., Deino, A., Drake, R. & Tesha, A. (1989) Chronology of Volcanism and Rift Basin Propagation- Rungwe Volcanic Province, East Africa. *Journal of Geophysical Research*, **94,** 15785-15803.

FOX, J., MC PHIE, J. & CAREY, R. (2016) Cape Grim, Nw Tasmania - a World Class Example of Submarine Basaltic Intraplate Volcanism. Australian Earth Sciences Convention, Adelaide.

GROVE, C. (2013) Submarine Hydrothermal Vent Complexes in the Paleocene of the Faroe-Shetland Basin: Insights from Three-Dimensional Seismic and Petrographical Data. *Geology*, **41,** 71-74.

HANSEN, D.M. (2006) The Morphology of Intrusion-Related Vent Structures and Their Implications for Constraining the Timing of Intrusive Events Along the Ne Atlantic Margin. *Journal of the Geological Society*, **163,** 789-800.

HOLFORD, S., SCHOFIELD, N., MACDONALD J.D, DUDDY I.R & P.F, G. (2007) Seismic Analysis of Igneous Systems in Sedimentary Basins and Their Impacts on Hydrocarbon Prospectivity: Examples from the Southern Australain Margin.

HOLFORD, S., SCHOFIELD, N., MACDONALD, J., DUDDY, I. & GREEN, P. (2012) Seismic Analysis of Igneous Systems in Sedimentary Basins and Their Impacts on Hydrocarbon Prospectivity: Examples from the Southern Australian Margin. *Australian Petroleum Production and Exploration Association Journal*, **52,** 229-252.

HOLT, S., HOLFORD, S. & FODEN, J. (2013) New Insights into the Magmatic Plumbing System of the South Australian Quaternary Basalt Province from 3d Seismic and Geochemical Data. *Australian Journal of Earth Sciences*, **60,** 797-817.

JACKSON, C.A.L. (2012) Seismic Reflection Imaging and Controls on the Preservation of Ancient Sill-Fed Magmatic Vents. *Journal of the Geological Society*, **169,** 503-506.

JAMTVEIT, B., SVENSEN, H., PODLADCHIKOV, Y.Y. & PLANKE, S. (2004) Hydrothermal Vent Complexes Associated with Sill Intrusions in Sedimentary Basins. *Physical geology of high-level magmatic systems*, **234,** 233-241.

Jerram, D.A. (2002) Volcanology and Facies Architecture of Flood Basalts. *Geological Society of America Special Papers*, **362,** 119-132.

Johnson, R.W. (1989) *Intraplate Volcanism in Eastern Australia and New Zealand*. Cambridge University Press.

Kokelaar, P. (1986) Magma-Water Interactions in Subaqueous and Emergent Basaltic. *Bulletin of Volcanology*, **48,** 275-289.

Magee, C., Briggs, F. & Jackson, C.A. (2013a) Lithological Controls on Igneous Intrusion-Induced Ground Deformation. *Journal of the Geological Society*, **170,** 853-856.

Magee, C., Hunt-Stewart, E. & Jackson, C.A.-L. (2013b) Volcano Growth Mechanisms and the Role of Sub-Volcanic Intrusions: Insights from 2d Seismic Reflection Data. *Earth and Planetary Science Letters*, **373,** 41-53.

Magee, C., Duffy, O.B., Purnell, K., Bell, R.E., Jackson, C.A.L. & Reeve, M.T. (2015) Fault-Controlled Fluid Flow Inferred from Hydrothermal Vents Imaged in 3d Seismic Reflection Data, Offshore Nw Australia. *Basin Research*, 20.

Maresh, J., White, R.S., Hobbs, R.W. & Smallwood, J.R. (2006) Seismic Attenuation of Atlantic Margin Basalts: Observations and Modeling. *Geophysics*, **71,** B211-B221.

McClintock, M., White, J.D.L., Houghton, B.F. & Skilling, I.P. (2008) Physical Volcanology of a Large Crater-Complex Formed During the Initial Stages of Karoo Flood Basalt Volcanism, Sterkspruit, Eastern Cape, South Africa. *Journal of Volcanology and Geothermal Research*, **172,** 93-111.

Meeuws, F., Holford, S., Foden, J. & Schofield, N. (2016) Distribution, Chronology and Causes of Cretaceous–Cenozoic Magmatism Along the Magma-Poor Rifted Southern Australian Margin: Links between Mantle Melting and Basin Formation. *Marine and Petroleum Geology*, **73**, 271-298.

Moore, J.G. (1985) Structure and Eruptive Mechanisms at Surtsey Volcano, Iceland. *Geological Magazine*, **122,** 649-661.

Muirhead, J.D., Eaton, A.R., Re, G., White, J.D.L. & Ort, M.H. (2016) Monogenetic Volcanoes Fed by Interconnected Dikes and Sills in the Hopi Buttes Volcanic Field, Navajo Nation, USA. *Bulletin of Volcanology*, **78,** 1-16.

Nelson, C.E., Jerram, D.A. & Hobbs, R.W. (2009) Flood Basalt Facies from Borehole Data: Implications for Prospectivity and Volcanology in Volcanic Rifted Margins. *Petroleum Geoscience*, **15,** 313-324.

Planke, S. & Eldholm, O. (1994) Seismic Response and Construction of Seaward Dipping Wedges of Flood Basalts: Vøring Volcanic Margin. *Journal of Geophysical Research: Solid Earth (1978–2012)*, **99,** 9263-9278.

Planke, S., Symonds, P.A., Alvestad, E. & Skogseid, J. (2000) Seismic Volcanostratigraphy of Large-Volume Basaltic Extrusive Complexes on Rifted Margins. *Journal of Geophysical Research*, **105,** 19335-19351.

Planke, S., Rasmussen, T., Rey, S. & Myklebust, R. (2005). Seismic Characteristics and Distribution of Volcanic Intrusions and Hydrothermal Vent Complexes in the Vøring and Møre Basins. *Geological Society, London, Petroleum Geology Conference series*, Geological Society of London. **6**, 833-844.

Rateau, R., Schofield, N. & Smith, M. (2013) The Potential Role of Igneous Intrusions on Hydrocarbon Migration, West of Shetland. *Petroleum Geoscience*, **19,** 259-272.

Re, G., White, J. & Ort, M.H. (2015) Dikes, Sills, and Stress-Regime Evolution During Emplacement of the Jagged Rocks Complex, Hopi Buttes Volcanic Field, Navajo Nation, USA. *Journal of Volcanology and Geothermal Research*, **295,** 65-79.

SAAR, M.O. & MANGA, M. (1999) Permeability-Porosity Relationship in Vesicular Basalts. *Geophys. Res. Lett.*, **26,** 111-114.

SCHOFIELD, N., HOLFORD, S., MILLETT, J., BROWN, D., JOLLEY, D., R. PASSEY, S., MUIRHEAD, D., GROVE, C., MAGEE, C., MURRAY, J., HOLE, M., A.-L. JACKSON, C. & STEVENSON, C. (2015) Regional Magma Plumbing and Emplacement Mechanisms of the Faroe-Shetland Sill Complex: Implications for Magma Transport and Petroleum Systems within Sedimentary Basins. *Basin Research***,** n/a-n/a.

SCHUTTER, S.R. (2003) Hydrocarbon Occurrence and Exploration in and around Igneous Rocks. *Geological Society, London, Special Publications*, **214,** 7-33.

SIGURDSSON, H., HOUGHTON, B., MCNUTT, S., RYMER, H. & STIX, J. (2015) *The Encyclopedia of Volcanoes*. Elsevier.

SUITING, I. & SCHMINCKE, H.-U. (2009) Internal Vs. External Forcing in Shallow Marine Diatreme Formation: A Case Study from the Iblean Mountains (Se-Sicily, Central Mediterranean). *Journal of Volcanology and Geothermal Research*, **186,** 361-378.

SUITING, I. & SCHMINCKE, H.U. (2012) Iblean Diatremes 3: Volcanic Processes on a Miocene Carbonate Platform (Iblean Mountains, Se-Sicily): A Comparison of Deep Vs. Shallow Marine Eruptive Processes. *Bulletin of Volcanology*, **74,** 207-230.

SUTHERLAND, F. & WELLMAN, P. (1986). Potassium-Argon Ages of Tertiary Volcanic Rocks, Tasmania. *Papers and Proceedings of the Royal Society of Tasmania*, **120**, 77-86.

SVENSEN, H., PLANKE, S., JAMTVEIT, B. & PEDERSEN, T. (2003) Seep Carbonate Formation Controlled by Hydrothermal Vent Complexes: A Case Study from the Vøring Basin, the Norwegian Sea. *Geo-Marine Letters*, **23,** 351-358.

Svensen, H., Planke, S., Malthe-Sorenssen, A., Jamtveit, B., Myklebust, R., Rasmussen Eidem, T. & Rey, S.S. (2004) Release of Methane from a Volcanic Basin as a Mechanism for Initial Eocene Global Warming. *Nature*, **429,** 542-545.

Svensen, H., Jamtveit, B., Planke, S. & Chevallier, L. (2006) Structure and Evolution of Hydrothermal Vent Complexes in the Karoo Basin, South Africa. *Journal of the Geological Society*, **163,** 671-682.

Svensen, H., Planke, S., Chevallier, L., Malthe-Sørenssen, A., Corfu, F. & Jamtveit, B. (2007) Hydrothermal Venting of Greenhouse Gases Triggering Early Jurassic Global Warming. *Earth and Planetary Science Letters*, **256,** 554-566.

Thomson, K. & Hutton, D. (2004) Geometry and Growth of Sill Complexes: Insights Using 3d Seismic from the North Rockall Trough. *Bulletin of Volcanology*, **66,** 364-375.

Thomson, K. (2007) Determining Magma Flow in Sills, Dykes and Laccoliths and Their Implications for Sill Emplacement Mechanisms. *Bulletin of Volcanology*, **70,** 183-201.

Thordarson, T. & Self, S. (1993) The Laki (Skaftár Fires) and Grímsvötn Eruptions in 1783–1785. *Bulletin of Volcanology*, **55,** 233-263.

Totterdell, J. & Bradshaw, B. (2004). *The Structural Framework and Tectonic Evolution of the Bight Basin*. Eastern Australasian Basins Symposium II. Petroleum Exploration Society of Australia, Special Publication, 41-61.

Trigg, K.R., Blevin, J.E. & Boreham, C. (2003) An Audit of Petroluem Wells in the Bass Basin 1965-1999, Geoscience Australia Record 2003/11 ISSN: 1039-0073.

Valentine, G.A. & Cortés, J.A. (2013) Time and Space Variations in Magmatic and Phreatomagmatic Eruptive Processes at Easy Chair (Lunar Crater Volcanic Field, Nevada, USA). *Bulletin of volcanology*, **75,** 1-13.

WALL, M., CARTWRIGHT, J., DAVIES, R. & MCGRANDLE, A. (2010) 3d Seismic Imaging of a Tertiary Dyke Swarm in the Southern North Sea, Uk. *Basin Research*, **22,** 181-194.

WATTON, T.J., JERRAM, D.A., THORDARSON, T. & DAVIES, R.J. (2013a) Three-Dimensional Lithofacies Variations in Hyaloclastite Deposits. *Journal of Volcanology and Geothermal Research*, **250,** 19-33.

WATTON, T.J., WRIGHT, K.A., JERRAM, D.A. & BROWN, R.J. (2013b) The Petrophysical and Petrographical Properties of Hyaloclastite Deposits: Implications for Petroleum Exploration. *AAPG Bulletin*, **98**, 449-463.

WHITE, J.D. & ROSS, P.-S. (2011) Maar-Diatreme Volcanoes: A Review. *Journal of Volcanology and Geothermal Research*, **201,** 1-29.

WRIGHT, K.A., DAVIES, R.J., JERRAM, D.A., MORRIS, J. & FLETCHER, R. (2012) Application of Seismic and Sequence Stratigraphic Concepts to a Lava-Fed Delta System in the Faroe-Shetland Basin, Uk and Faroes. *Basin Research*, **24,** 91-106.

ZHAO, F., WU, S., SUN, Q., HUUSE, M., LI, W. & WANG, Z. (2014) Submarine Volcanic Mounds in the Pearl River Mouth Basin, Northern South China Sea. *Marine Geology*, **355,** 162-172.

Fig. 1. (a) Location map of the Labatt and Yolla surveys in the Basin Basin. Bathymetric contours are in metres. (b) Map showing the distribution of Eocene-Recent-aged basalts, onshore southern Australia. Modified from Johnson, R. W., 1989. (c) Stratigraphic column, also showing seismic horizons picked in this study.

Fig. 2. 2D seismic line (a) and interpretation (b) connecting the Labatt and Yolla surveys.

Fig. 3. Seismic section showing the correlation between seismic data and the Yolla-1 and Bass-1 wells. Adapted from Trigg, K. R. *et al.* (2003).

Fig. 4. Time map of the TV2 and TV1 surfaces in the Labatt (a) and Yolla (b) surveys.

Fig. 5. Seismic line and interpretation through the Labatt survey. See Fig. 4 for location. TV2=Top Volcanic, BV2=Base Volcanic, EVCM= Eastern View Coal Measures.

Fig. 6. Seismic line and interpretation through the Yolla survey. See Fig. 4 for location. TV1=Top Volcanic, BV1=Base Volcanic, EVCM= Eastern View Coal Measures.

Fig. 7. Seismic sections and interpretive sketches of crater–type (a), pointed (b), flat-topped (c) and cratered (d) vents. See Fig. 4 for their location. Graphs (e) and (f) show the relationship between vent volume and height and basal diameter for the cone-type vents.

Fig. 8. Seismic cross section of a vent fed by a sill. TV2=Top Volcanic, BV2=Base Volcanic. See Fig. 4 for location.

Fig. 9. Schematic diagram showing the evolution of the volcanoes from pit craters (maars) (a), to pointed-types (pillow volcanoes) (b) and finally cratered and flat-topped types (tuff cones) (c).

Fig. 10. Seismic cross section of a hydrothermal vent (a) located on the Northeast Atlantic margin. An increase in acoustic impedance is represented by a blue reflection. Modified from Schofield, N. *et al.*, 2015. (b) Seismic cross section from a volcano in this study. A red reflection represents an increase in acoustic impedance. See Fig. 4 for location.

Table 1. Compilation of well data showing the volcanic intervals found in Bass Basin exploration wells. Compiled from Blevin, J. (2003) and Trigg, K. R. *et al.*, (2003).

Table 2. Summary of the morphology of the vents osberved in this study.

Table 3. Characteristics of vent structures observed in seismic data. [(1)] Compiled from Planke, S. *et al.* 2005; Hansen, D. M., 2006; Svensen, H. *et al.*, 2006 and Grove, C., 2013. [(2)] From Magee, C. *et al.*, 2013b. [(3)] From Wall, M. *et al.* 2010. [(4)] From Bell, B. & Butcher, H., 2002. *calculated using depths in time from Planke, S. *et al.* 2005 and a velocity of 3 km s^{-1}

Well	Depth below KB volcanic material intersected (m)	Water depth (m)	KB elevation (m)	Description	Inferred age
Aroo-1	3150−3600	76	9.8	Weathered basaltic flows interbedded with sandstones	Late Cretaceous to Palaeocene
Bass-1	790−950	81	No data	Pyroclastic material	Miocene
Bass-2	1679−1757	85	No data	Intrusion	Unknown
Chat-1	>3000	81	25	Volcanics	Late Cretaceous to Palaeocene
Cormorant-1	2450−2600	73	30	Volcanics and olivine gabbro sill	Miocene
Durroon-1	1584−1591; 1542−1645	68	10	Volcaniclastic sandstone	Early Cretaceous
Flinders-1	2200−2290	69	No data	Dolerite intrusion	Miocene
Koorkha-1	2100−2140	67	22	Basaltic intrusion	Eocene
Seal-1	1500−1600; >1650	64	25	Dolerite intrusion	Miocene
Silvereye-1	As metre-thick intervals between 1290−1425 and 2110−2300	54	No data	Altered, blocky volcanics, possibly of pyroclastic origin, also dolerite	Eocene
Squid-1	2350−2390	80	22	Alkali olivine basalt intrusion	Unknown
Tasmanian Devil-1	>750	74	22	Basalts	Palaeocene
Tilana-1	1250−1400 2000−2250 >3100	79	22	Vesicular basalt; gabbro; basalt	Mid Eocene to Mid Oligocene; Early to Mid Eocene; Late Maastrichtian to Late Palaeocene
Toolka-1	2400−2700	78	9	Intrusion	Unknown
Yolla-1	1237−1305; >3000	79	11	Highly altered pyroclastics; doleritic intrusion	Miocene ; Late Cretaceous to Palaeocene

Table 1

Vent morphology		n	Crater diameter (km)	Diameter (km)	Height (km)	Volume (km^3)
Crater-type	Crater	15	n/a	0.3–1.2	n/a	n/a
Cone type	Pointed	7	n/a	1–3	0.13–0.16	0.4–1.1
	Cratered	5	380–950	3–5	0.2–0.31	0.07–1.36
	Flat-topped	7	n/a	1–4	0.12–0.52	1–1.4

Table 2.

Vent type	Basal D (km)	Height (km)	Depth to underlying sill (km)	Dyke fed?	Morphology	Dominant lithology	Spatial Distribution	Basal relationship	Timing of emplacement	Internal reflections
Hydrothermal [(1)]	0.4−1 1	0.03−0.45	300−650 0*	No	Crater, eye or dome shaped	Diatomitic siltstone, carbonate and sandstone	Linear rows or isolated	Flat-lying concordant, downwarped concordant, truncated	Dominantly synchronous, pre-dating main stage of effusive activity	Chaotic, and low-moderate amplitude, sub-parallel reflections which downlap the pre-eruptive surface
Shield volcano [(2)]	1.94−18.89	0.02− 1	0.05− 1.5	Yes	Cone-shaped with rounded or flat tops	Hyaloclastite, lava flows, interbedded sediments and minor intrusions	Linear rows or isolated	Upwarped concordant, flat-lying concordant	Not described	Chaotic, and low-high amplitude, sub-parallel reflections which downlap the pre-eruptive surface
Maar [(3)]	0.2−1	Not described	N/A	Yes	Crater shaped	N/A	Linear rows	Truncated	Synchronous	Low-moderate amplitude, sub-parallel reflections which onlap crater wall
Seamount [(4)]	≤2	>0.1	Not described	Not described	Cone-shaped	Pillow lava and hyaloclastite	Above sills	Flat-lying concordant	Not described	Low-high amplitude reflections which downlap the pre-eruptive surface
Tuff cones, pillow volcanoes and maars (this study)	0.3−5	0.12−0.52	495−120 0	Yes	Cone-shaped with cratered, flat topped or pointed morphologies, also crater-shaped	Pyroclasts and hyaloclastite	Linear rows or isolated	Upwarped concordant, truncated	Diachronous	Chaotic, and moderate-high amplitude, hummocky reflections which downlap the pre-eruptive surface

Table 3.

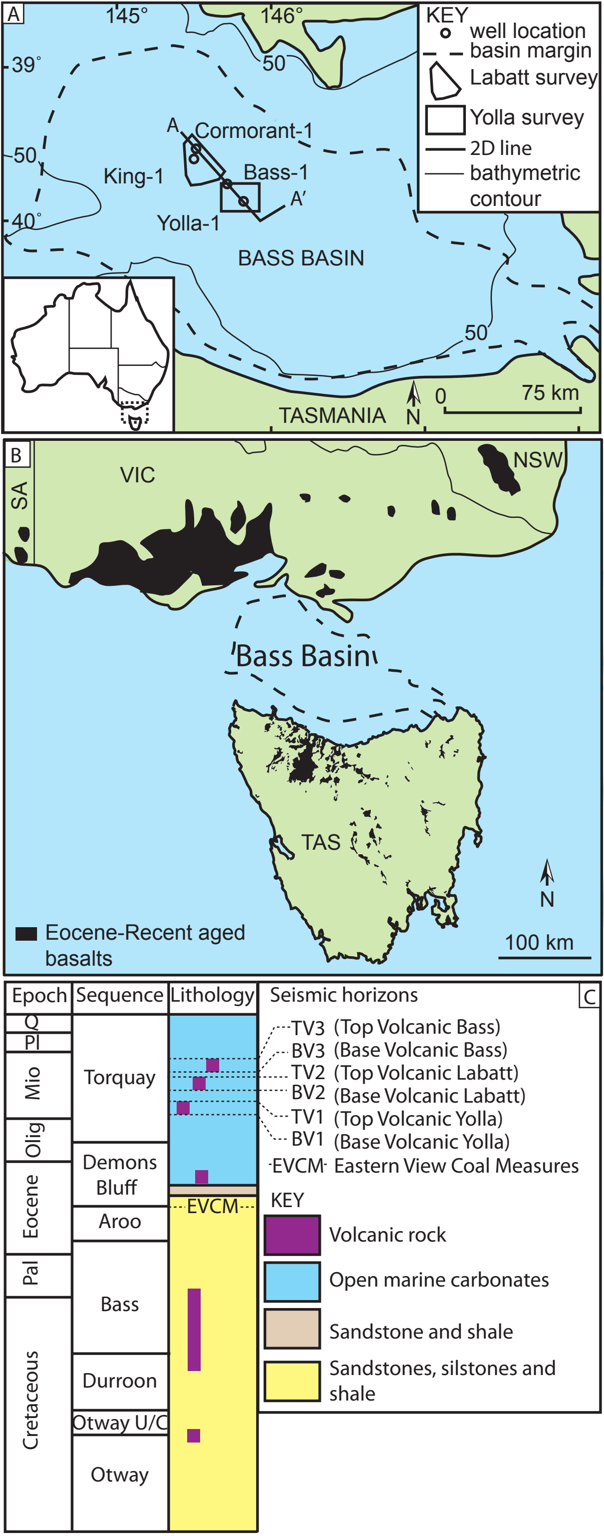
A
145°
146°
39°
50
KEY
well location
basin margin
Labatt survey
Yolla survey
2D line
bathymetric contour
A
Cormorant-1
King-1
Bass-1
A′
Yolla-1
50
40°
BASS BASIN
50
0
75 km
N
TASMANIA
B
VIC
NSW
SA
Bass Basin
TAS
N
Eocene-Recent aged basalts
100 km
Epoch
Sequence
Lithology
Seismic horizons
C
Q
Pl
Mio
Olig
Eocene
Pal
Cretaceous
Torquay
Demons Bluff
Aroo
Bass
Durroon
Otway U/C
Otway
EVCM
TV3 (Top Volcanic Bass)
BV3 (Base Volcanic Bass)
TV2 (Top Volcanic Labatt)
BV2 (Base Volcanic Labatt)
TV1 (Top Volcanic Yolla)
BV1 (Base Volcanic Yolla)
EVCM Eastern View Coal Measures
KEY
Volcanic rock
Open marine carbonates
Sandstone and shale
Sandstones, silstones and shale

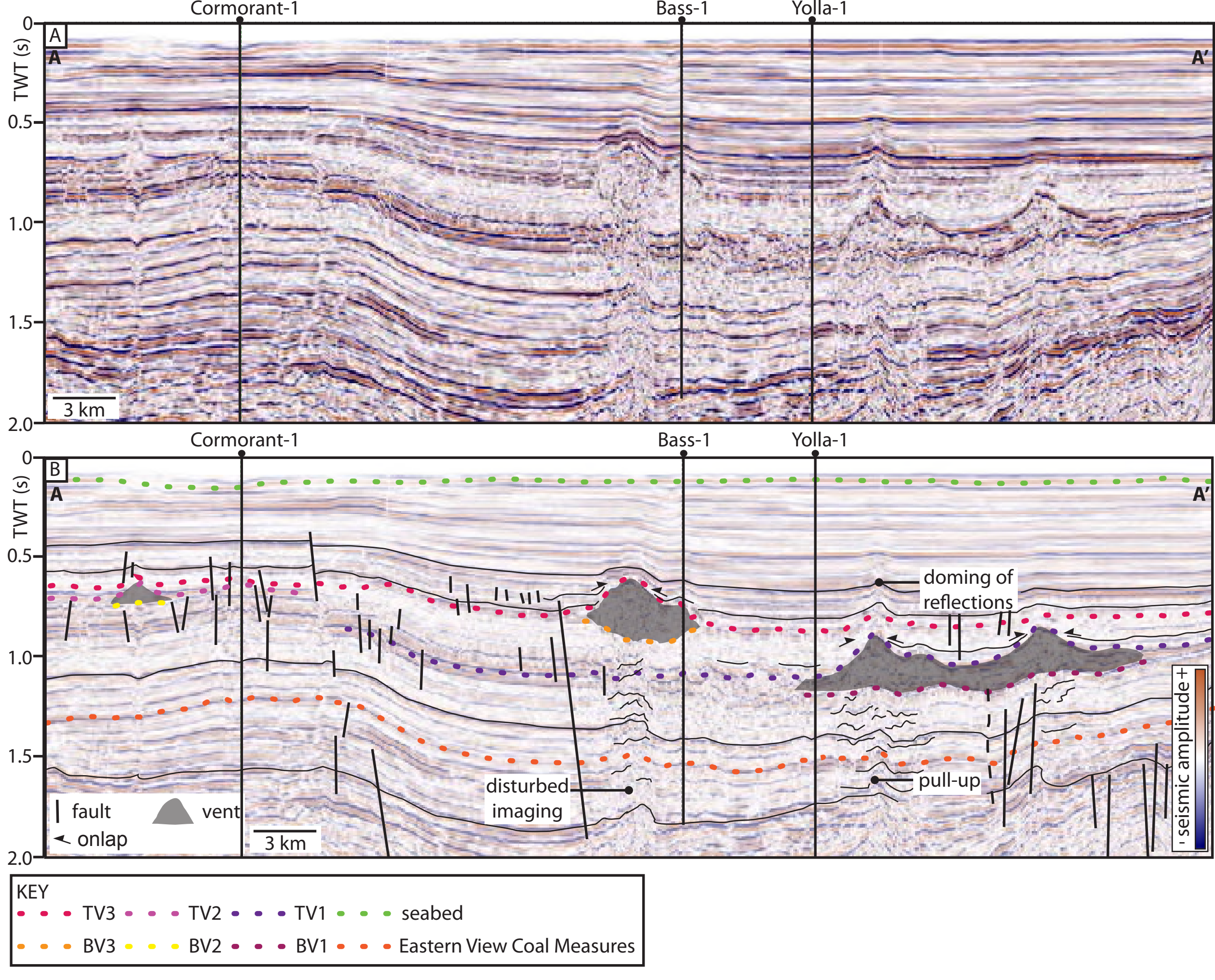

Cormorant-1
Bass-1
Yolla-1
A
TWT (s)
A
A'
0
0.5
1.0
1.5
2.0
3 km
B
doming of reflections
disturbed imaging
pull-up
fault
vent
onlap
seismic amplitude
KEY
TV3
TV2
TV1
seabed
BV3
BV2
BV1
Eastern View Coal Measures

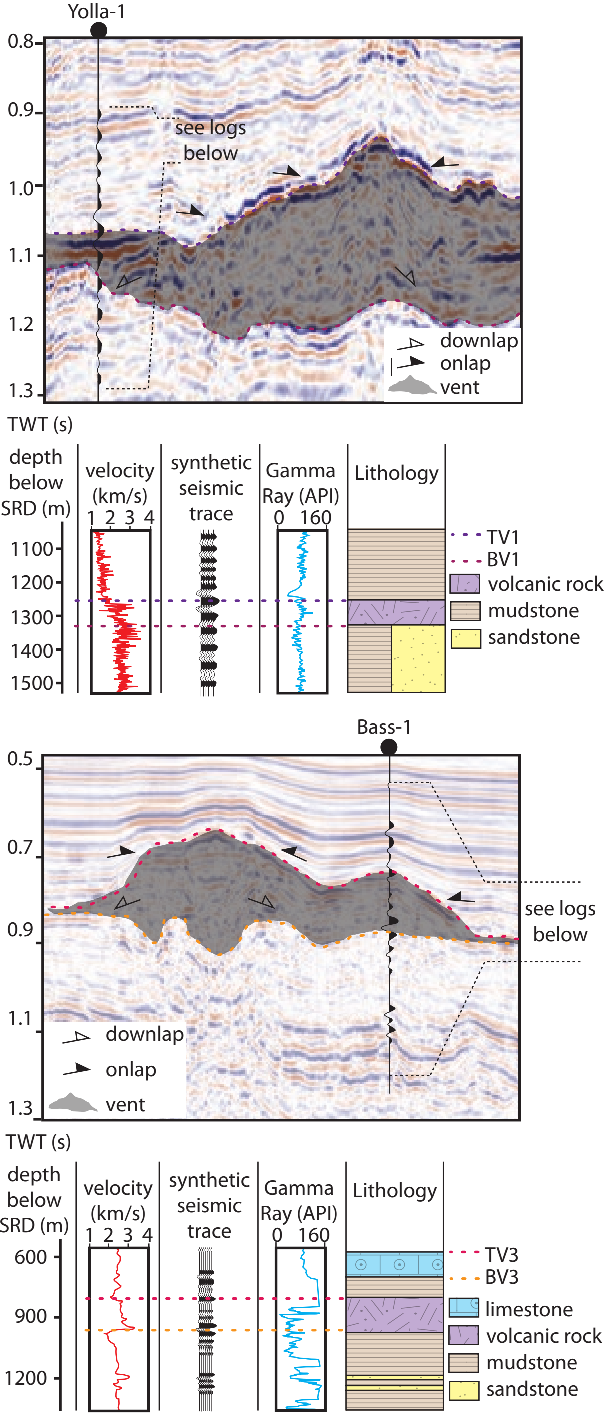

Yolla-1
0.8
0.9
1.0
1.1
1.2
1.3
TWT (s)
see logs below
downlap
onlap
vent
depth below SRD (m)
1100
1200
1300
1400
1500
velocity (km/s)
1 2 3 4
synthetic seismic trace
Gamma Ray (API)
0 160
Lithology
TV1
BV1
volcanic rock
mudstone
sandstone
Bass-1
0.5
0.7
0.9
1.1
1.3
TWT (s)
see logs below
downlap
onlap
vent
depth below SRD (m)
600
900
1200
velocity (km/s)
1 2 3 4
synthetic seismic trace
Gamma Ray (API)
0 160
Lithology
TV3
BV3
limestone
volcanic rock
mudstone
sandstone

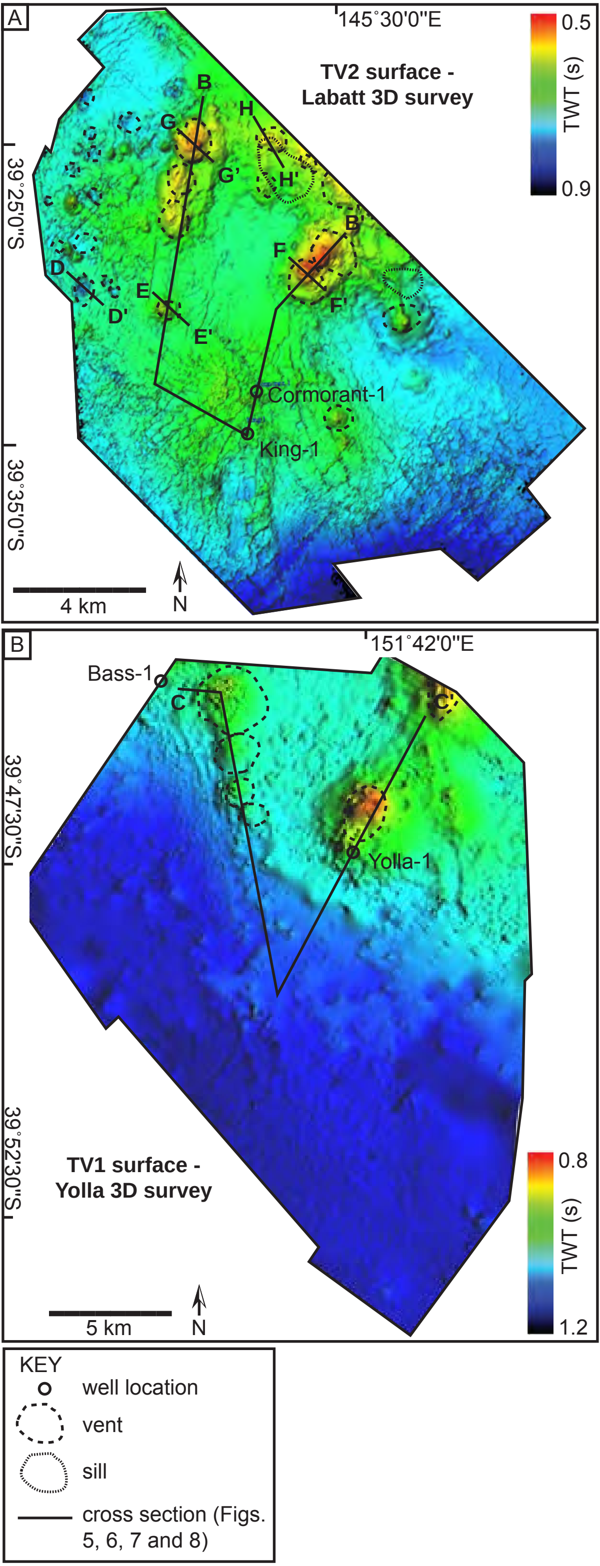
A
145°30'0"E
TV2 surface - Labatt 3D survey
0.5
TWT (s)
0.9
B
G
G'
H
H'
B'
F
F'
D
D'
E
E'
Cormorant-1
King-1
39°25'0"S
39°35'0"S
4 km
N
B
151°42'0"E
Bass-1
C
C'
Yolla-1
39°47'30"S
39°52'30"S
TV1 surface - Yolla 3D survey
0.8
TWT (s)
1.2
5 km
N
KEY
well location
vent
sill
cross section (Figs. 5, 6, 7 and 8)

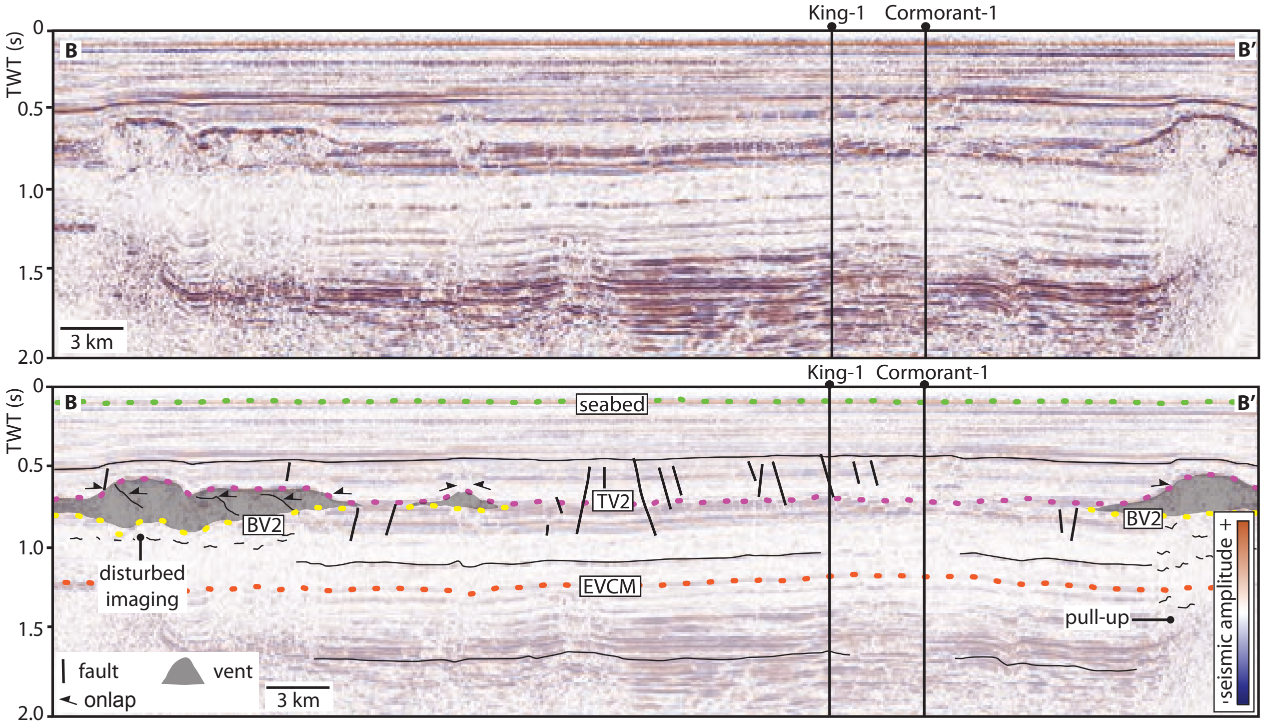
King-1
Cormorant-1
TWT (s)
0
0.5
1.0
1.5
2.0
B
B′
3 km
King-1
Cormorant-1
TWT (s)
0
0.5
1.0
1.5
2.0
B
B′
seabed
TV2
BV2
BV2
disturbed imaging
EVCM
pull-up
fault
vent
onlap
3 km
- seismic amplitude +

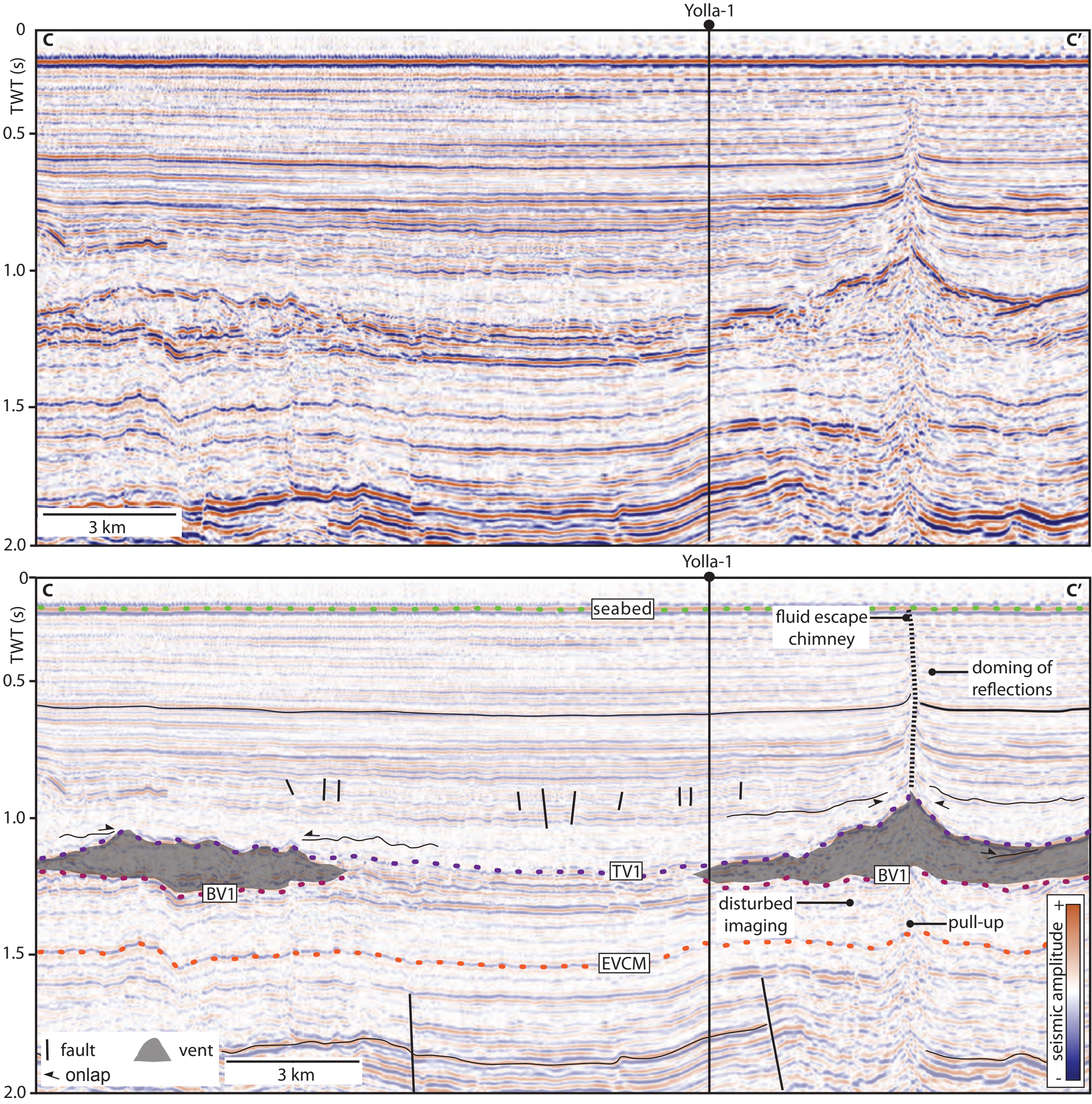

Yolla-1
C
C'
TWT (s)
0
0.5
1.0
1.5
2.0
3 km
Yolla-1
C
C'
seabed
fluid escape
chimney
doming of
reflections
TV1
BV1
BV1
disturbed
imaging
pull-up
EVCM
fault
onlap
vent
3 km
seismic amplitude
+
-

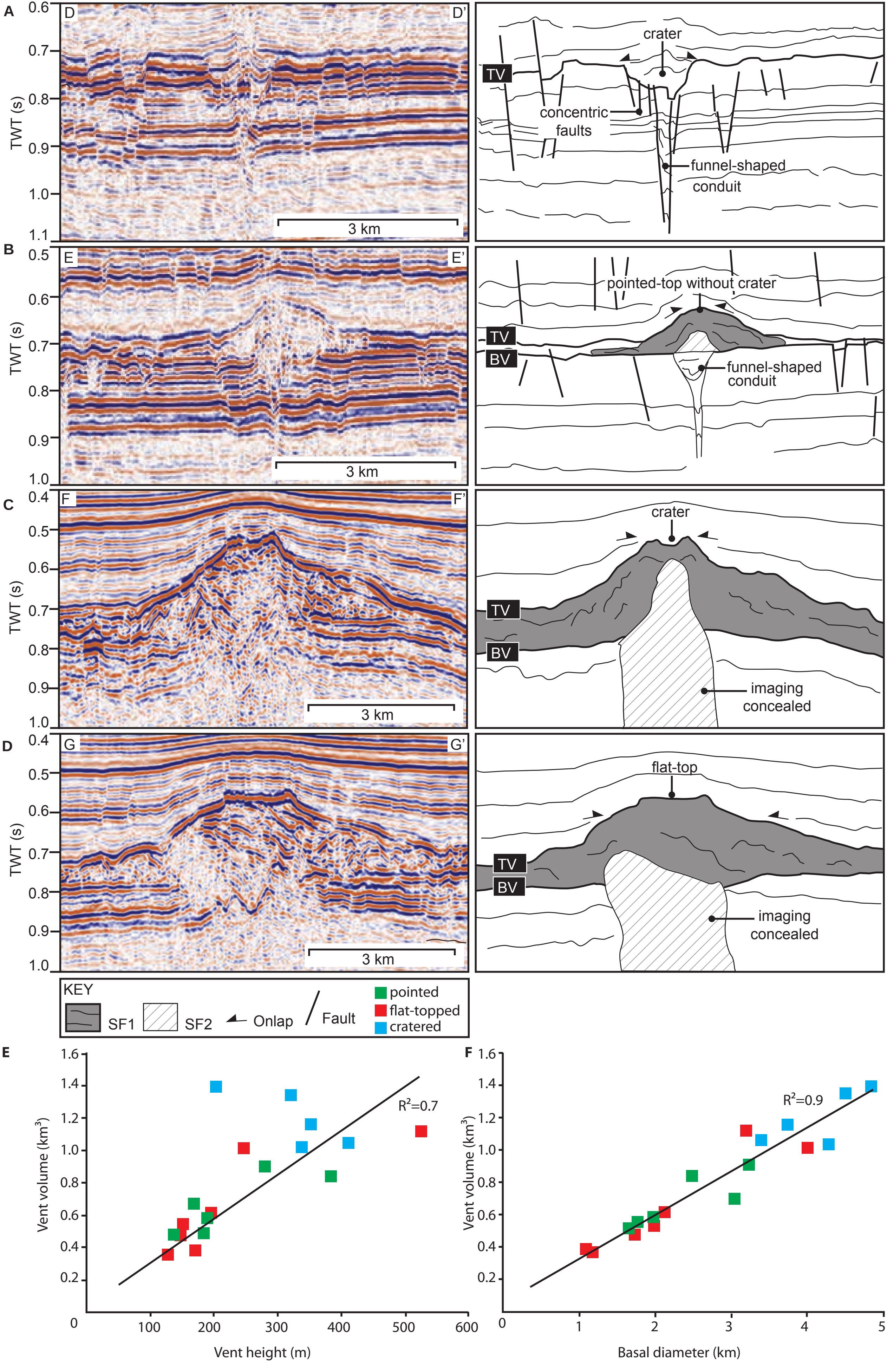

A
B
C
D
E
F
TWT (s)
D
D'
E
E'
F
F'
G
G'
3 km
crater
TV
BV
concentric faults
funnel-shaped conduit
pointed-top without crater
imaging concealed
flat-top
KEY
SF1
SF2
Onlap
Fault
pointed
flat-topped
cratered
Vent volume (km³)
Vent height (m)
Basal diameter (km)
R²=0.7
R²=0.9

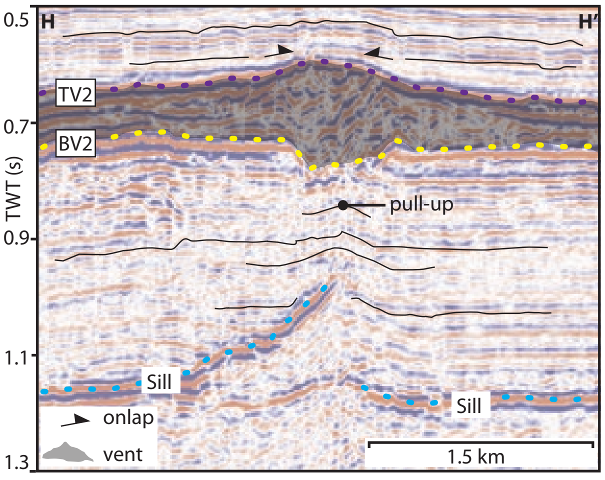
H
H'
0.5
0.7
0.9
1.1
1.3
TWT (s)
TV2
BV2
pull-up
Sill
Sill
onlap
vent
1.5 km

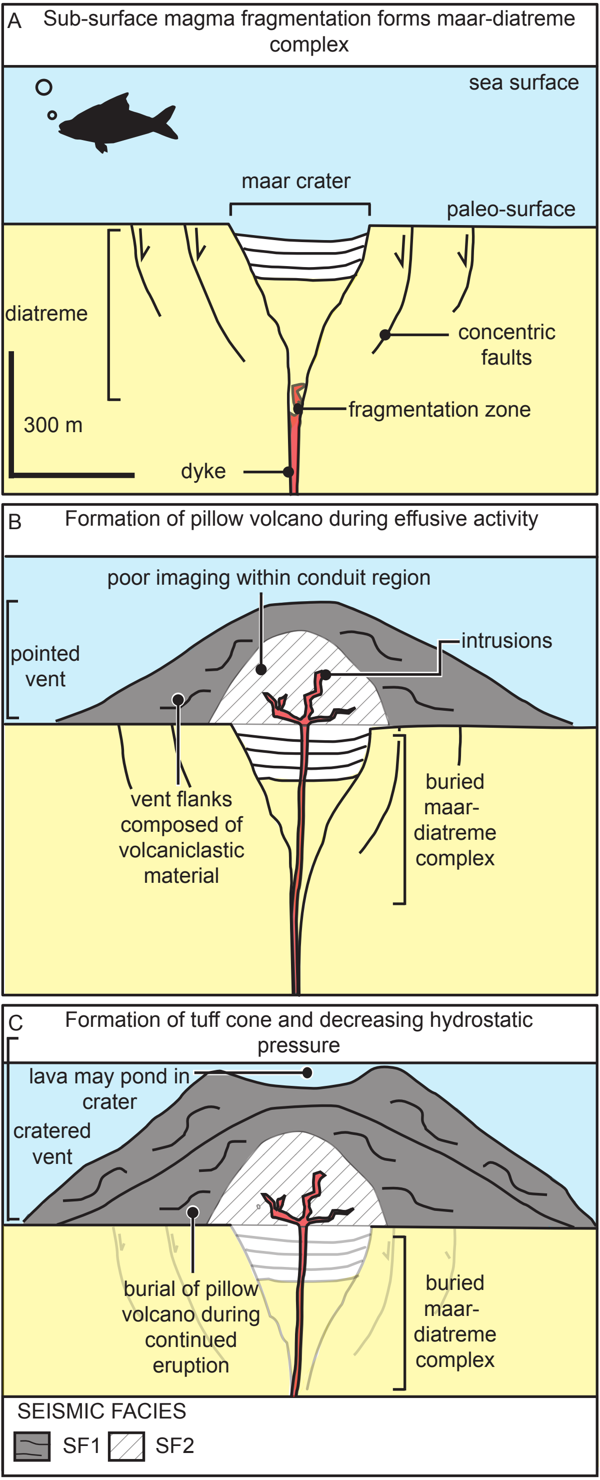
A
Sub-surface magma fragmentation forms maar-diatreme complex
sea surface
maar crater
paleo-surface
diatreme
concentric faults
300 m
fragmentation zone
dyke
B
Formation of pillow volcano during effusive activity
poor imaging within conduit region
pointed vent
intrusions
vent flanks composed of volcaniclastic material
buried maar-diatreme complex
C
Formation of tuff cone and decreasing hydrostatic pressure
lava may pond in crater
cratered vent
burial of pillow volcano during continued eruption
buried maar-diatreme complex
SEISMIC FACIES
SF1
SF2

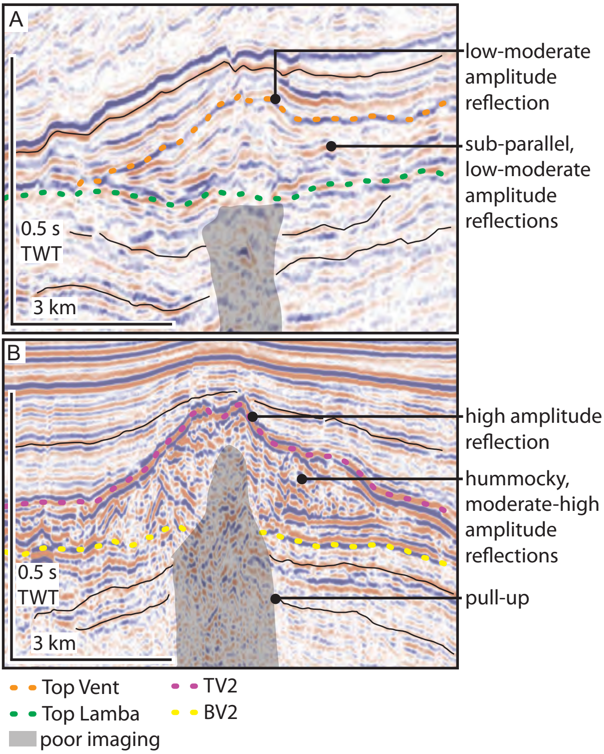
A
B
low-moderate amplitude reflection
sub-parallel, low-moderate amplitude reflections
0.5 s TWT
3 km
high amplitude reflection
hummocky, moderate-high amplitude reflections
pull-up
0.5 s TWT
3 km
Top Vent
Top Lamba
poor imaging
TV2
BV2